energies

MDPI

Article

Energy Performance Evaluation of a Ventilated Façade System through CFD Modeling and Comparison with International Standards

Sofia Pastori [1,*], Riccardo Mereu [2], Enrico Sergio Mazzucchelli [1], Stefano Passoni [2] and Giovanni Dotelli [3]

[1] Department of Architecture, Built environment and Construction engineering, Politecnico di Milano, 20133 Milan, Italy; enrico.mazzucchelli@polimi.it
[2] Department of Energy, Politecnico di Milano, 20156 Milan, Italy; riccardo.mereu@polimi.it (R.M.); stefano.passoni@polimi.it (S.P.)
[3] Department of Chemistry, Materials and Chemical Engineering "Giulio Natta", Politecnico di Milano, 20133 Milan, Italy; giovanni.dotelli@polimi.it
* Correspondence: sofia.pastori@polimi.it

Abstract: Ventilated façades can help to reduce summer building thermal loads and, therefore, energy consumption due to air-conditioning systems thanks to the combined effect of the solar radiation reflection and the natural or forced ventilation into the cavity. The evaluation of ventilated façades behavior and performance is complex and requires a complete thermo-fluid dynamic analysis. In this study, a computational fluid dynamic (CFD) methodology has been developed for the complete assessment of the energy performance of a prefabricated timber–concrete composite ventilated façade module in different operating conditions. Global numerical results are presented as well as local ones in terms of heat flux, air velocity, and temperature inside the façade cavity. The results show the dependency of envelope efficiency on solar radiation, the benefits that natural convection brings on potential energy savings and the importance of designing an optimized façade geometry. The results concerning the façade behavior have been thoroughly compared with International Standards, showing the good accuracy of the model with respect to these well-known procedures. This comparison allowed also to highlight the International Standards procedures limits in evaluating the ventilated façade behavior with the necessary level of detail, with the risk of leading to design faults.

Keywords: CFD; ventilated façade; energy efficiency; natural ventilation; forced ventilation; timber construction

Citation: Pastori, S.; Mereu, R.; Mazzucchelli, E.S.; Passoni, S.; Dotelli, G. Energy Performance Evaluation of a Ventilated Façade System through CFD Modeling and Comparison with International Standards. *Energies* **2021**, *14*, 193. https://doi.org/10.3390/en14010193

Received: 21 November 2020
Accepted: 28 December 2020
Published: 1 January 2021

1. Introduction

Energy efficiency and sustainability in the building sector are necessary to achieve the 2030 Agenda for Sustainable Development Goals [1], since the construction industry is one of the major industries responsible for climate change and global waste production. For this reason, the use of passive solutions—such as ventilated façades, lightweight construction, and sustainable materials—is gaining importance within the building design strategies.

Passive solutions, such as high energy-efficient building envelopes, have a primary role in reaching a greater sustainability, improving thermal comfort and indoor climatic conditions without energy consumption, thanks to a reasonable building orientation and an optimal thermal performance [2]. Among them, ventilated façades can help to reduce summer thermal loads due to direct solar radiation [3], thanks to the radiation reflection (using high-reflection-coefficient paints [4]), and to the cavity natural or forced ventilation [5].

Many studies have been carried out in order to analyze heat and mass transfer through the building envelope, also regarding timber walls, even if there is a lack of research related to the energy assessment of timber–concrete composite façades.

Timber is a hygroscopic material, therefore its thermal conductivity is dependent from its moisture content. Simo-Tagne et al. [6] developed a coupled one-dimensional

heat and mass transfer model to simulate the hygrothermal flux through five tropical woods used as building walls in sub-Saharan African region, after integration of outdoor conditions. They found that wood type, wall thickness, climatic seasons, air temperature and relative humidity influence the coupled heat and mass transfer through the wall, while material cutting direction had no influence. They also underlined the importance of protecting the wood to prevent the wall deterioration because of moisture content. Danovska et al. [7] evaluated the uncertainty introduced in building energy simulation codes by adopting nominal timber thermal properties without considering the dependence on material temperature and moisture content. The thermal behavior of a 30 cm CLT (cross-laminated timber) wall was simulated using a 1D finite difference model calibrated against experimental results and considering the typical reference years of 110 Italian locations. Their results showed that the adoption of nominal thermal conductivity instead of the variable one including the moisture brings to an underestimation between 1% and 3% of the hourly heat fluxes for the tested *CLT* wall. Destro et al. [8] studied a timber–concrete composite prefabricated wall system, similar to the one analyzed in the present study, but without ventilated air gap. They performed hot-box measures for the evaluation of the system thermal resistance (following ISO 8990:1994), varying the delta temperature between the two wall sides and neglecting moisture influence. The experimental tests were then used to calibrate FEM models and to compare the results with the standard directives.

Regarding the thermal behavior of ventilated facades, several studies have been conducted using 2D numerical models, even if such studies are lacking for timber–concrete composite systems.

The detailed assessment of the energy performance of ventilated façades is a constantly current issue in research since their interaction with the external environment is really complex and requires an in-depth fluid dynamic analysis of the air flow inside the cavity or experimental tests. Souza et al. [9] conducted a CFD analysis on a naturally ventilated façade to assess the effectiveness of its installation. They simulated different solar radiation conditions and used the numerical results to visualize the local flow-field inside the cavity. By benchmarking against experimental results, they assessed the accuracy of the numerical approach used. Zhang et al. in [10] were able to test the influence of geometrical parameters on the natural ventilation inside vertical air cavity typical of double-skin façades thanks to CFD. The simulations allowed the authors to test the effect of cavity width and height on induced flowrate, heat flux, temperature, and velocity profiles and, in the end, they were able to provide design guidelines. Coussirat et al. in [11] evaluated instead the influence of numerical models for convection, radiation and turbulence on the performance estimation of a ventilated façade. From their analysis, it is worth noting that the k-e family turbulence modeling is suitable for this kind of problems. Blocken et al. in [12] investigated the possibility of decoupling the numerical simulation of the ventilated envelope by modeling the building with closed cavities and then the cavities separately. They showed how this approach leads to an important overestimation of the air change rate per hour, thus advising for coupled simulation of both the environment and the cavity together.

In this research, a model for the assessment of the energy performance of a prefabricated ventilated façade module during the hot season was developed, using a 3D CFD (computational fluid dynamics) approach. The results have been compared with International Standards UNI EN ISO 6946, used for ventilated façade design, and ISO 15099 which refers to double skin façades, but it can also be applied to opaque ventilated façades. The CFD analysis allowed the evaluation of both fluid motion and heat transfer yielding global and local results, as well as the possibilities of examining the façade performance in different operating conditions and thus increasing the accuracy and modularity of new designs. The effects of moisture content were not considered in the model, since the research objective is the comparison between CFD and International Standards UNI EN ISO 6946 [13] and ISO 15099 [14], which do not consider the envelope hygrometric behavior. Furthermore, coherently with previous studies, where it was shown the limited contribution of the moisture effect on timber–concrete walls thermal modeling [7,8], it was

neglected in order to simplify the model from a computational point of view. Anyway, the studied wall is not subject to condensation problems, also thanks to the cavity ventilation which allows to remove moisture and condensation, especially during winter.

The comparison with international standards was useful to verify the CFD results consistency in absence of experimental results and also to highlight the simplified procedures weakness in evaluating a ventilated façade behavior with the necessary level of detail, with the consequent risk of design faults.

2. Materials and Methods

2.1. Opaque Ventilated Façade System Choice and Description

For the construction of modern energy-efficient buildings, lightweight construction is becoming very popular among designers. European Union (EU) legislation encourages such design, especially if wood, as a sustainable material, is used [15]. Engineered wood products have been gaining larger consensus within the construction market in the last years and they are more often being preferred to diffused and traditional construction materials, as sustainable and greatly performing alternatives in the realization of buildings [16,17]. Contraction of scheduling is one of the main reasons why, in the timber construction field, advanced prefabricating systems are consistently gaining market share [18,19].

The analyzed system is a prefabricated panel made of an external concrete slab coupled to a timber-frame panel [20] (Figure 1). Between the timber frame panel and the concrete slab, a ventilated air cavity is located. Once the prefabricated panels are installed, a counter-wall for building services integration purposes and for hiding the panels geometric tolerances is built. The counter-wall was not considered in the analysis presented below, since its characteristics (thickness and materials) may change. Moreover, the counter-wall contributes to the envelope thermal transmittance reduction but does not influence the behavior of the ventilated cavity, that is mostly affected by the external climatic conditions. The façade layers characteristics are shown in Table 1.

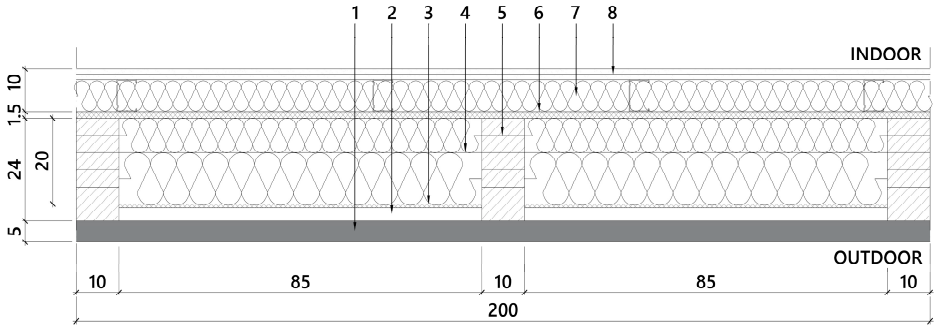

Figure 1. Horizontal section of the opaque ventilated façade module analyzed. The layers numbering refers to Table A1.

Table 1. Opaque ventilated façade layers description [21,22].

Layer	Thickness d (m)	Thermal Conductivity λ (W/mK)	Density ρ (kg/m^3)
1. Reinforced concrete slab	0.050	2.0	2400
2. Ventilated air cavity	0.031	Variable	Variable
3. OSB panel	0.015	0.10	550
4. Timber frame	0.240	0.13	385
5. Rockwool	0.200	0.035	100
6. OSB panel	0.009	0.10	600
7. Thermal insulated cavity for services integration	0.075	0.035	40
8. Double gypsum plasterboard	0.025	0.210	900

The common timber-frame solutions are characterized by the wide use of insulating material and by a reduced amount of timber [23]. They have an optimal thermal behavior in winter, but they can be less performing in summer because they are characterized by a low thermal inertia [24]. The studied system combines the characteristic of a timber-frame panel with a reinforced concrete slab in order to optimize the energy performance in summer.

As it can be seen in Figure 1, the posts of the timber-frame panel, which also support the reinforced concrete slab, divide the cavity into continuous vertical compartments for the entire height of the façade and their width depends on the distance of the posts. The distance considered in the case study is 85 cm. The air can enter the ventilation cavity through a system of underground ducts, connected to external air intake wells, and can exit at the top of the façade (Figure 2). The air flow in the cavity is a natural motion triggered by the thermal gradient (chimney effect) or, just in case, forced by dedicated electric fans. The thermo-fluid dynamic analysis presented considers only one of the cavities of the façade in order to reduce the computational cost of the simulation by exploiting the periodicity of the system, as shown in Figure 2.

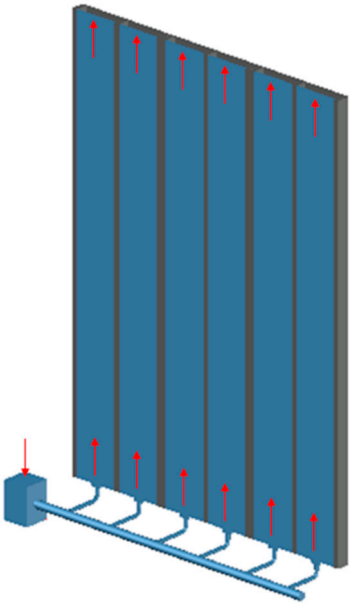

Figure 2. Functional scheme of the opaque ventilated façade.

2.2. Mathematical Model

Considered the state of the art in the simulation of natural convection in vertical channels presented in the introduction, the approach used in this work is a steady-state Reynolds-averaged Navier–Stokes (RANS) one with a two-equation turbulence model and where the solution of continuity, radiation, heat transfer, and turbulence model equations occur in a coupled way. A brief explanation of the solving equation is reported below (more details in [25]).

2.2.1. Continuity

$$\frac{\partial}{\partial x_i}(\rho u_i) = 0 \tag{1}$$

2.2.2. Momentum Conservation

$$\frac{\partial}{\partial x_j}(\rho u_i u_j) = -\frac{\partial p}{\partial x_i} + \frac{\partial}{\partial x_j}\left[\mu\left(\frac{\partial u_i}{\partial x_j} + \frac{\partial u_j}{\partial x_i} - \frac{2}{3}\delta_{ij}\frac{\partial u_j}{\partial x_i}\right)\right] + \frac{\partial}{\partial x_j}\left(-\rho\overline{u_i' u_j'}\right) \tag{2}$$

where ρ is the air density, p is the air pressure, and μ its dynamic viscosity.

2.2.3. Energy Conservation

$$\nabla\cdot\left(\vec{v}(\rho E+p)\right)=\nabla\cdot\left(k_{eff}\,\nabla T-\sum_{j}h_j\vec{J_j}+\left(\bar{\bar{\tau}}_{eff}\cdot\vec{v}\right)\right)+S_h \quad (3)$$

where k_{eff} is the effective conductivity (sum of material and turbulent thermal conductivity), $\vec{J_j}$ is the diffusion flux of species j and E is the total energy defined as $E=h-\frac{p}{\rho}+\frac{v^2}{2}$.

2.2.4. Turbulence Model

The realizable k-ε model relies on transport equations for k (turbulent kinetic energy) and e (turbulence dissipation)

$$\frac{\partial}{\partial x_j}\left(\rho k u_j\right)=\frac{\partial}{\partial x_j}\left[\left(\mu+\frac{\mu_t}{\sigma_k}\right)\frac{\partial k}{\partial x_j}\right]+G_K+G_b-\rho\varepsilon-Y_M+S_K \quad (4)$$

$$\frac{\partial}{\partial x_j}\left(\rho\varepsilon u_j\right)=\frac{\partial}{\partial x_j}\left[\left(\mu+\frac{\mu_t}{\sigma_\varepsilon}\right)\frac{\partial\varepsilon}{\partial x_j}\right]+\rho C_1 S\varepsilon-\rho C_2\frac{\varepsilon^2}{k+\sqrt{\nu\varepsilon}}+C_{1\varepsilon}\,\frac{\varepsilon}{k}\,C_{3\varepsilon}\,G_b+S_E \quad (5)$$

In these equations, G_K represents the source term of turbulence kinetic energy due to the mean velocity gradients, G_b represents the one due to buoyancy, Y_M is the contribution of the fluctuating dilatation in compressible turbulence to the overall dissipation rate, $C_{1\varepsilon}$ and C_2 are calibration constants while S_K and S_E are user-defined source terms. σ_k and σ_ε are instead the turbulent Prandtl numbers for k and ε, respectively.

2.2.5. Radiation Model

The DO Model radiative transfer equation (RTE) solved is

$$\nabla\cdot\left(I\left(\vec{r},\vec{s}\right)\vec{s}\right)+(a+\sigma_s)I\left(\vec{r},\vec{s}\right)=an^2\frac{\sigma T^4}{\pi}+\frac{\sigma_s}{4\pi}\int_0^{4\pi}I\left(\vec{r},\vec{s}\right)\Phi\left(\vec{s}\cdot\vec{s}\right)d\Omega' \quad (6)$$

where I is the radiation intensity that depends on position and direction, a and σ_s the absorption and scattering coefficients respectively, n is the refractive coefficient and Φ represents the phase function.

2.3. Physical Model

2.3.1. Geometrical Model

The fluid dynamic analysis has been carried out in a 3D geometrical domain to properly reproduce the façade system geometry and to simulate the full tri-dimensional velocity field. The geometrical model represents the fluid domain where air flows through the duct and the cavity of the façade. The cavity has a height of 8.5 m, a width of 0.85 m and a depth of 0.031 m, while the underground duct has been reproduced as a straight pipe with diameter of 0.08 m and length of 1 m. The geometry of the top of the cavity simulates the air flow deviation due to the flashing, installed on site on the top of the façade [20].

The other façade layers (concrete slab and timber-frame wall) are not geometrically represented but modeled through a 1D approach that allows to consider the thermal properties and the thickness of the materials, without heavily increasing the computational cost.

The façade has been modeled with the same geometry for all the operating conditions tested in the study, the only difference relies in the presence of the air volume at the inlet (inlet domain) of the underground duct, necessary to simulate the surrounding environment for the natural ventilation case [26]. This volume is not required in case of forced ventilation, where an air velocity value is imposed at the underground duct inlet. Both models include another air volume (outlet domain) for the simulation of the external environment at the top of the cavity. The volumes dimensions are 0.25 m^3 for the inlet

domain (equal to the ventilated cavity volume) and 0.67 m^3 for the outlet domain. Figure 3 shows the 3D geometrical models used for the natural and forced ventilation simulations.

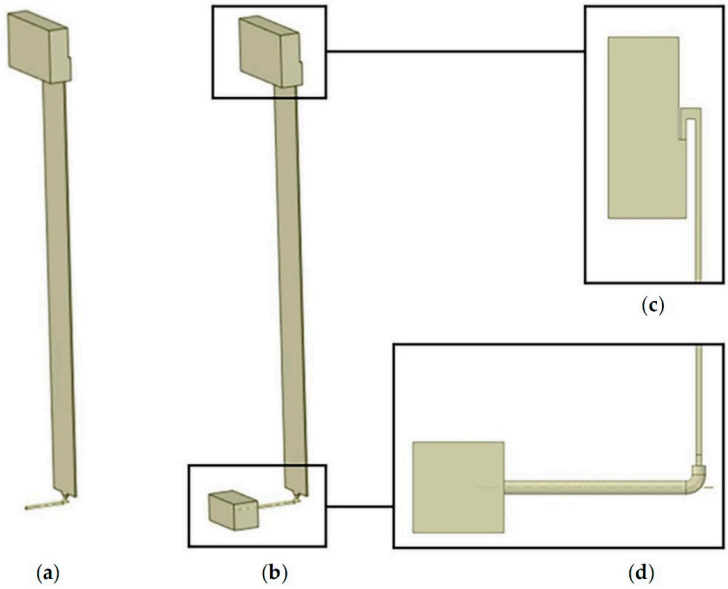

Figure 3. Model geometry for forced (**a**) and natural (**b**) ventilation. Details (**c**,**d**)show respectively the inlet and the outlet domain.

2.3.2. Mesh

The spatial discretization of the numerical domain is realized by a polyhedral mesh composed of 400,000 cells (Figure 4). This mesh type allows to discretize complex geometries limiting the cell skewness, reproducing the gradients with high quality and limiting the numerical diffusivity. The cells size ranges between 15 and 50 mm, coherently with the size of the cavity and the duct, while the presence of the mesh boundary layer is ensured along all the walls in order to correctly catch the viscous layer effects [27]. The cell skewness and grow rate are limited to 0.6 and 1.2 respectively, in order to increase the accuracy of the numerical solution. A sensitivity analysis on the mesh size influence has been carried out by evaluating the numerical solution on different meshes ranging from 400,000 (coarse) to 1.2 million cells (fine). The quantity chosen as benchmark is the thermal power extracted by ventilation. It has been noticed that this quantity exhibits a change of 1.12% from the coarse to the fine mesh, and considering the increment in computational time, this suggests that the adopted mesh is of sufficiently high resolution.

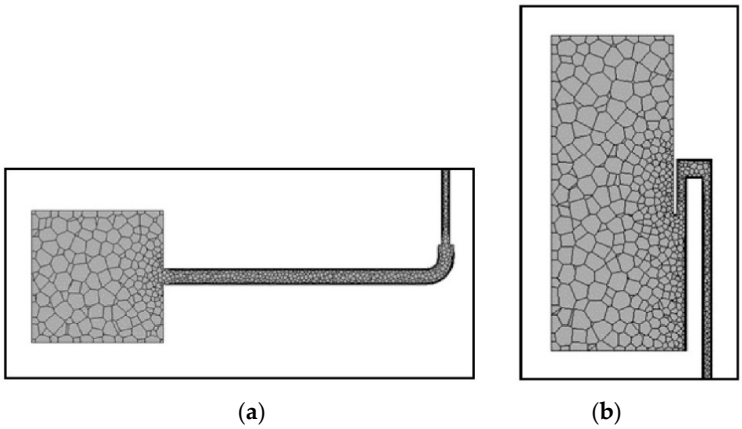

Figure 4. Vertical sections of the inlet (**a**) and outlet (**b**) volumes mesh.

2.3.3. Boundary Conditions

The boundary conditions of the numerical model for both fluid dynamic and thermal quantities are reported and briefly described below.

Outdoor Environment

The thermal boundary conditions used for the simulations [28] refer to Budoni (Sardinia, Italy). The hourly weather conditions are represented by the sol-air temperature T_{sa}, a single variable that includes both the external air temperature and the solar radiation

$$T_{sa} = T_e + \frac{\alpha I}{h_e} \quad (7)$$

where:

- T_e = maximum value of external air temperature during summer [°C];
- I = maximum value of solar incident radiation on vertical surfaces during summer [W/m^2];
- α = absorption coefficient of the external surface of the façade;
- h_e = external convective-radiative heat transfer coefficient, equal to 25 W/m^2K. This conventional value is commonly used [3,27,29,30] and it allows a simplification of the CFD model, avoiding the modeling of the external natural convection and radiation. Moreover, it is needed to make a direct comparison with the international standards calculation procedures, according to the study purpose.

The sol–air temperature values have been calculated for each hour and orientation (south, east, north, west), considering both α = 0.8 and α = 0.4, in order to evaluate the influence of the external surface color on the façade energy performance (sensitivity analysis). The study presented in this article refers only to the west orientation, as it is the one with the most critical climatic conditions during summer (highest T_{sa} values), as shown in Table A1 (Appendix A).

Indoor Environment

The indoor air temperature and the internal convective-radiative heat transfer coefficient have been considered respectively equal to 26 °C and 7.7 W/m^2K [29].

Inlet and Outlet Domains

The boundary conditions imposed at the inlet and at the outlet refer to the air temperature T_e and the static pressure $P_s = P_0 + \rho gh$ (wind pressure is not considered) [27]. In the forced ventilation case, the air velocity at the duct inlet is imposed equal to its maximum value obtained in the natural ventilation case all over the day, in order to evaluate the effect of the 'best natural ventilation conditions' on the façade over the day. The velocity has been kept at that threshold value to limit the fan energy consumption and to make a comparison with the natural ventilation case.

Façade and Underground Duct

The façade surfaces are modeled considering the *no slip* condition along them. All the surfaces not facing the indoor or the outdoor environment are set up as adiabatic (no heat flux through them).

The underground duct surface is also modeled considering the no slip condition. During summer the ground surrounding the duct has a temperature lower than outdoor air. In this case, the duct is positioned at −0.50 m underground, hence a temperature equal to $T_e - 2.5$ °C [31] has been imposed on the duct surface. This allows to evaluate the air cooling per meter through the duct.

2.3.4. Numerical Set-Up

The simulations have been run using the finite-volume solver ANSYS Fluent release 2019 R3. The properties of the materials assigned to the model (air, concrete, timber, and rockwool), operating conditions, models and numerical methods used are reported in Tables A2 and A3 Appendix A.

3. Results and Discussion

In this section, a comprehensive analysis of thermo-fluid dynamic behavior of the façade with no ventilation (closed cavity), natural ventilation and forced ventilation into the cavity through CFD approach and comparison with international standard procedures is reported. Furthermore, a sensitivity analysis varying the solar absorption coefficient (α) is performed. Initially, it is assumed equal to 0.8 concerning a 15-h time slot, from 7:00 a.m. to 10:00 p.m., when the external temperature is higher than the internal one, resulting in a positive heat flux entering the building. The sensitivity analysis considers halved value, α = 0.4 (for the cases with ventilated cavity only), instead, for only 4 h, when the incident solar radiation is the highest and the influence of the absorption coefficient is the most relevant. All the simulations performed are listed in Table 2.

Table 2. Summary of the CFD simulations performed.

Façade Behavior		Solar Absorption Coefficient α	Time Interval
Unventilated façade	Closed air cavity	0.8	7:00 a.m.–10:00 p.m. (hourly step)
Ventilated façade	Natural ventilation	0.8	7:00 a.m.–10:00 p.m. (hourly step)
		0.4	12:00 a.m., 2:00 p.m., 4:00 p.m., 6:00 p.m.
	Forced ventilation	0.8	7:00 a.m.–10:00 p.m. (hourly step)
		0.4	12:00 a.m., 2:00 p.m., 4:00 p.m., 6:00 p.m.

3.1. Global Results

Global results concern the entire façade module performance assessment. The mean relative error (MRE) is introduced in order to calculate the statistical difference between the results given by CFD and the international standard considered

$$\text{MRE}\ (\%) = \frac{100}{N}\sum_{i=1}^{N}\frac{\left|P_{IS_i} - P_{CFD_i}\right|}{P_{IS_i}}$$

where P_{IS_i} and P_{CFD_i} are the values of the physical parameter studied (thermal resistance, heat flux, temperature or air velocity) given respectively by the international standard ISO 15099 or UNI EN ISO 6946 and by CFD simulations, i is the time of the day and N is the time slot considered.

The relative error (RE) of the CFD simulations with respect to the considered standard at each hour is shown in the graphs reported in the following. The RE was not calculated when the value of the physical parameter studied given by the standard tends to zero, because this leads to an increase of the relative error without physical meaning.

3.1.1. Unventilated Façade

The aim of the closed cavity simulation is to compare the thermal resistance value obtained from the CFD analysis with the one provided by the international standards, in order to benchmark the heat transfer sub-models set in Fluent by comparing the results.

The numerical value of thermal resistance (R_g) is calculated by dividing the area-weighted average temperature difference (ΔT) between the two faces of the cavity by the specific heat flux through the cavity itself (Q_{nv}). The R_g values obtained at every hour are then compared with those derived from the normative UNI EN ISO 6946 and ISO 15099, considering the same boundary conditions. The closed cavity thermal resistance

calculation procedure according to UNI EN ISO 6946 and ISO 15099 is described in the following paragraph.

The thermal resistance of the closed cavity (R_g) can be written as

$$R_g = \frac{1}{h_{cv} + h_{rd}} \quad (8)$$

where h_{cv} is the conduction/convection coefficient and h_{rd} the radiation coefficient.

According to UNI EN ISO 6946, the conduction/convection coefficient for closed vertical cavities is calculated by a simplified method: h_{cv} is the maximum between 1.250 W/m^2K and 0.025/d, where d is the cavity depth [29]. The Standard ISO 15099 suggests a more detailed procedure for the heat transfer calculation in closed vertical cavities [30], where h_{cv} depends on the Rayleigh number (and therefore on the air thermophysical properties, such as density, thermal conductivity, dynamic viscosity, thermal expansion coefficient, and specific heat at constant pressure), and on the delta temperature between the vertical cavity faces. According to both Standards, the radiation coefficient can be written as follows [31]:

$$h_{rd} = \frac{4\,\sigma\,T_m{}^3}{\frac{1}{\varepsilon_1} + \frac{1}{\varepsilon_2} - 1} \quad (9)$$

where σ is the Stefan–Boltzmann constant; T_m is the average thermodynamic temperature of the surfaces involved in the radiative heat exchange; and ε_1, ε_2 are the hemispherical emissivities of the external and internal surface of the cavity.

All the numerical results are resumed in Table 4. The discrepancy between the results provided by the standards is directly proportional to the delta temperature between the walls delimiting the cavity, due to the variation of temperature and incident solar radiation over the day. In fact, with the rise in ΔT, ISO 15099 considers an increase in convection effect into the cavity, while UNI EN ISO 6946 neglects it assuming still air and thus linking the air thermal resistance values only to the cavity thickness. The MRE between the results obtained by UNI EN ISO 6946 and by CFD is 8%.

The results obtained from the CFD simulations and those calculated in accordance with ISO 15099 are comparable, with a MRE of 2% between the values (Figure 5). This confirms the accuracy of the chosen heat transfer sub-model, which is then used for the simulations concerning ventilated configurations.

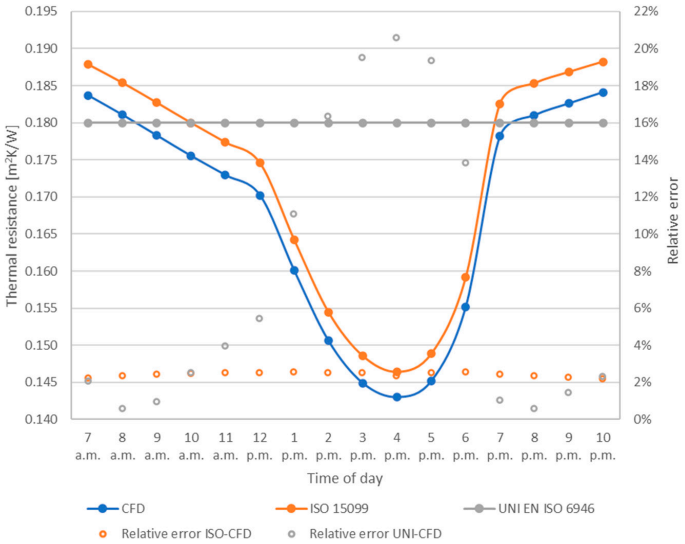

Figure 5. Comparison between the hourly thermal resistance values for the closed cavity provided by the CFD simulations and following the ISO 15099 and UNI EN ISO 6946 calculation procedures. The graph shows also the RE of the CFD results compared with the standards at each hour.

3.1.2. Ventilated Façade

The analysis considering natural ventilation allows to evaluate the influence of the external climatic conditions on the façade behavior over the day. Natural ventilation is driven by the pressure difference between the inlet and the outlet of the ventilated cavity, influenced by both the façade height and the temperature difference between the inside and the outside of the cavity, which varies during the day.

Figures 6 and 7 display how the air velocity and flow rate reflect the sol–air temperature profile, with a faster growth and the maximum peak in the hottest hours, and a semi-linear profile before 12:00 a.m. and after 7:00 p.m. This trend is related to the solar radiation, which significantly affects the temperature of the concrete slab, heating up the air in the cavity and then increasing the ventilation flow rate.

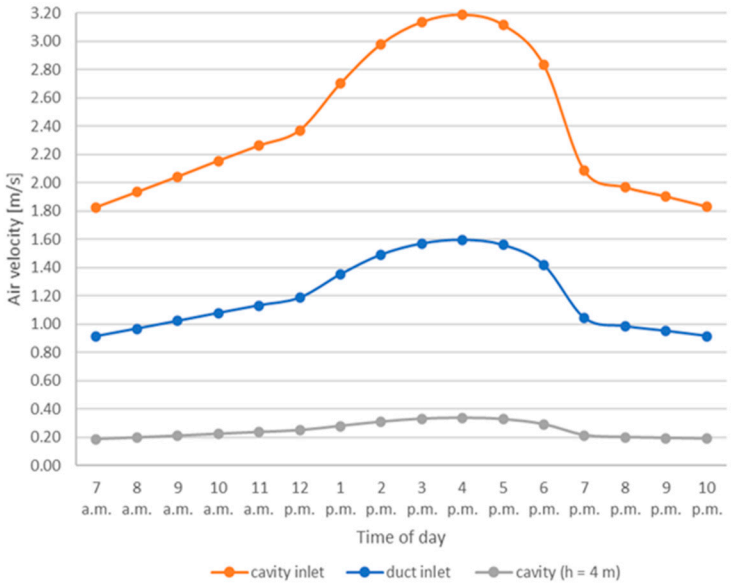

Figure 6. Hourly air velocity values referred to: duct inlet section, cavity inlet section (at the bottom of the façade), cross section of the cavity at a height of 4 m.

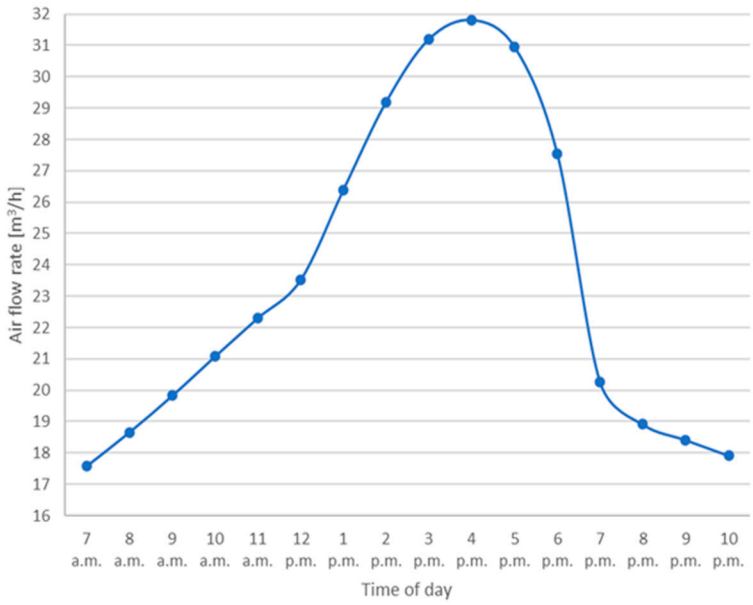

Figure 7. Hourly air flow rate through the naturally ventilated cavity.

The profiles shown in Figure 8, representing the heat fluxes $Q_{ext,n}$ (entering the cavity

from the external environment), $Q_{v,n}$ (removed from the cavity by natural ventilation), and $Q_{int,n}$ (flowing from the cavity to the indoor environment), have a shape similar to those of Figures 6 and 7, reaching the peak during the hottest hours of the day. All the heat fluxes presented in this study were calculated by dividing the rate of heat flow by the area of the ventilated façade (7.26 m^2). Therefore, the results presented can be intended as specific to 1 m^2 of heat exchanging surface.

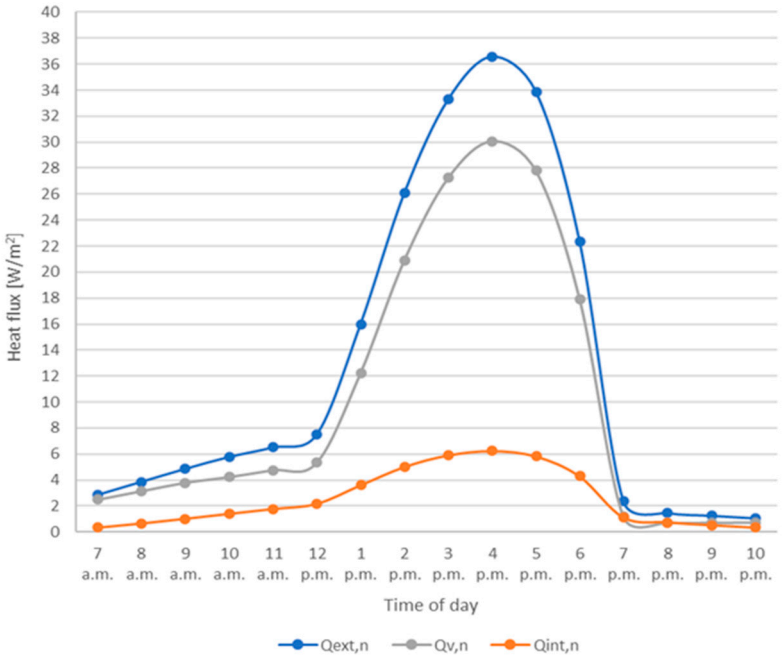

Figure 8. Hourly heat flux profiles obtained using the naturally ventilated façade: $Q_{ext,n}$ is the heat flux coming from the external environment into the cavity, $Q_{v,n}$ is the one removed by ventilation, and $Q_{int,n}$ is the heat flux that flows from the cavity to the internal environment.

In accordance with the air flow rate trend, the heat flux removed from the ventilated cavity reaches the peak values when the incident solar radiation is maximum. This means that, in case of low incident solar radiation, due to the façade exposure or to an overcast sky, the ventilated façade is much less efficient.

In the analysis concerning forced ventilation, a specific air velocity value was imposed, while the other boundary conditions are coincident with those used for natural ventilation. A constant air velocity value over the day was set on the inlet section of the underground duct, equal to the maximum value obtained in the natural ventilation case, i.e., 1.6 m/s (at 4 p.m. and $\alpha = 0.8$). Consequently, the air velocity and the flow rate in the cavity are constant over the day and are equal to 0.32 m/s and 30 m^3/h, respectively.

By comparing the heat fluxes that enter the building in case of forced ventilation ($Q_{int,f}$) and natural ventilation ($Q_{int,n}$), it is possible to quantify the benefit provided by forcing the air into the cavity with different velocities. Figure 9 shows the hourly reduction of Q_{int} obtained using forced ventilation instead of natural ventilation for the case analyzed, considering the same boundary conditions: the blue columns indicate the percentage reduction in the heat flux ($1\text{-}Q_{int,f}/Q_{int,n}$), while the orange lines show the difference $Q_{int,n}–Q_{int,f}$ (W/m^2).

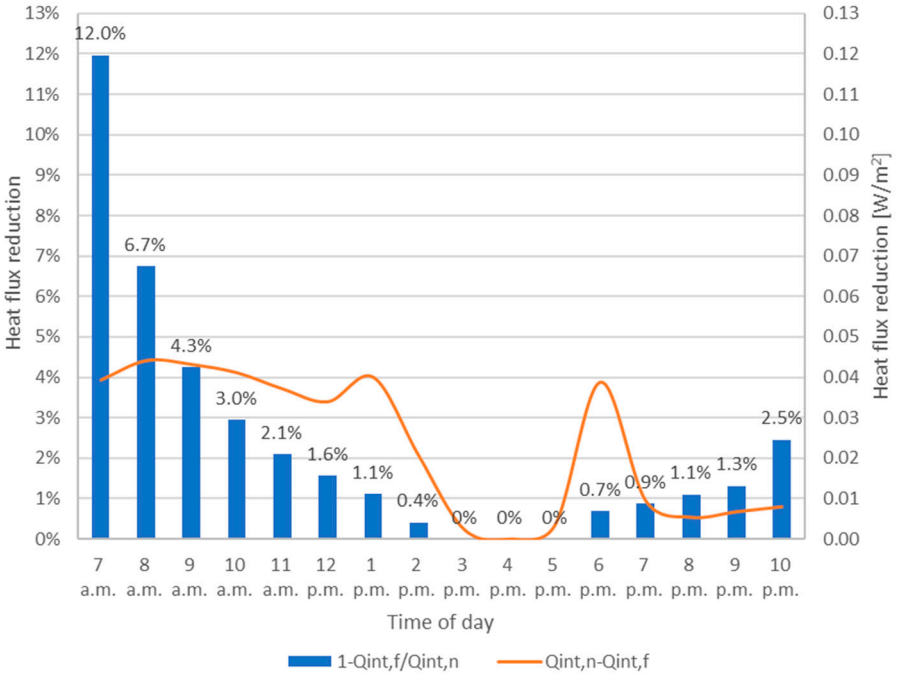

Figure 9. Hourly reduction of the heat flux entering the building provided by using forced ventilation ($Q_{int,f}$) instead of natural ventilation ($Q_{int,n}$).

As previously done in the case of closed cavity, the results obtained were compared with those provided by the Standards UNI EN ISO 6946 and ISO 15099. First of all, the heat flux $Q_{int,n}$ obtained from the CFD analysis was compared with the one obtained following the simplified calculation method proposed by UNI EN ISO 6946 for well-ventilated air layers [29], which requires the calculation of the ventilated façade thermal transmittance (described in Table 5 Appendix A). The values obtained show a good level of agreement, with a maximum difference of about 1 W/m^2 at 4 p.m., as it can be seen in Figure 10, and a MRE of CFD with respect to the standard equal to 11%. The increasing difference between the values calculated during the hottest hours of the day is due to the simplified method assumptions: the standard considers the presence of the ventilated cavity exclusively using a fictitious thermal resistance value (0.130 m^{2}K/W) constant over the day, thus neglecting the increase in the ventilation efficiency and in the heat flux removal during the afternoon hours, considered by CFD instead.

In order to make a comparison between the CFD and the ISO 15099 Standard, as previously done with UNI EN ISO 6946, a calculation procedure, explained in the following, was developed. The heat flux $Q_{int,n}$ calculated according to UNI EN ISO 6946, being consistent with the CFD results, was used as a starting point for the calculation of the air velocity and the heat flux removed $Q_{v,n}$ through ISO 15099. The values calculated were then compared with those obtained by the CFD simulations. The use of the heat flux values from UNI EN ISO 6946 is necessary because some input data (experimental data) are required by ISO 15099 in order to calculate the air velocity into the cavity and the heat flux removed by natural ventilation. The $Q_{int,n}$ values were not taken from the CFD results in order to keep the procedure independent from the fluid-dynamic simulations. The calculation procedure and the numerical results obtained are described in Appendix A, while Figures 11–13 show the comparison between the values from ISO 15099 and those provided by the CFD analysis.

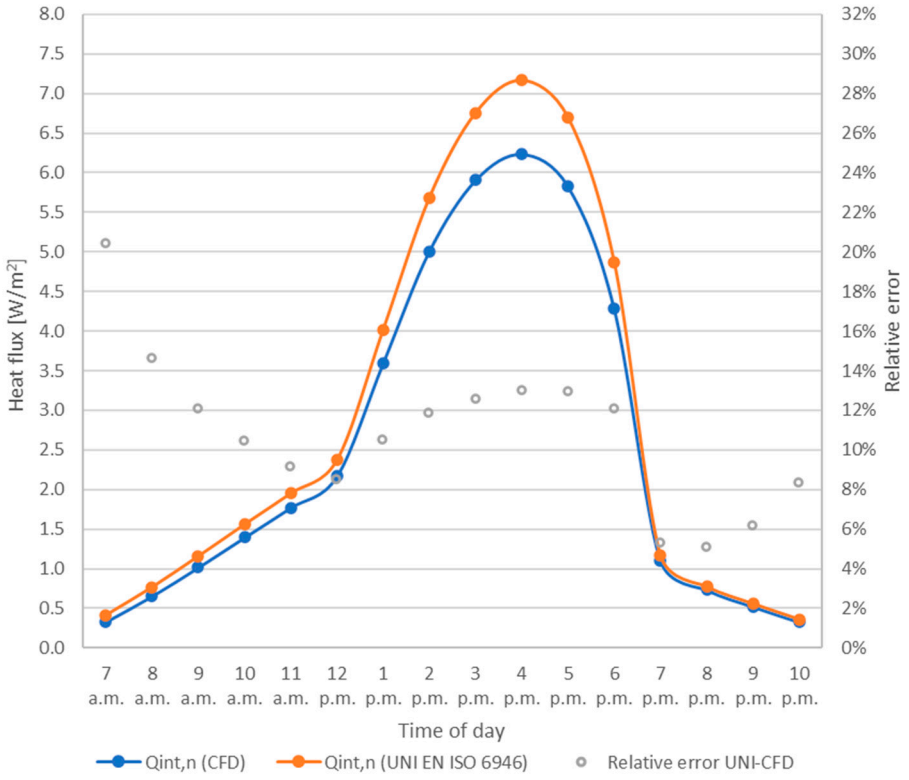

Figure 10. Comparison between the heat flux $Q_{int,n}$ obtained from the CFD analysis and the one calculated following the UNI EN ISO 6946 procedure referred to a well-ventilated air layer. The figure shows also the RE of the CFD results compared to the mentioned Standard at each hour.

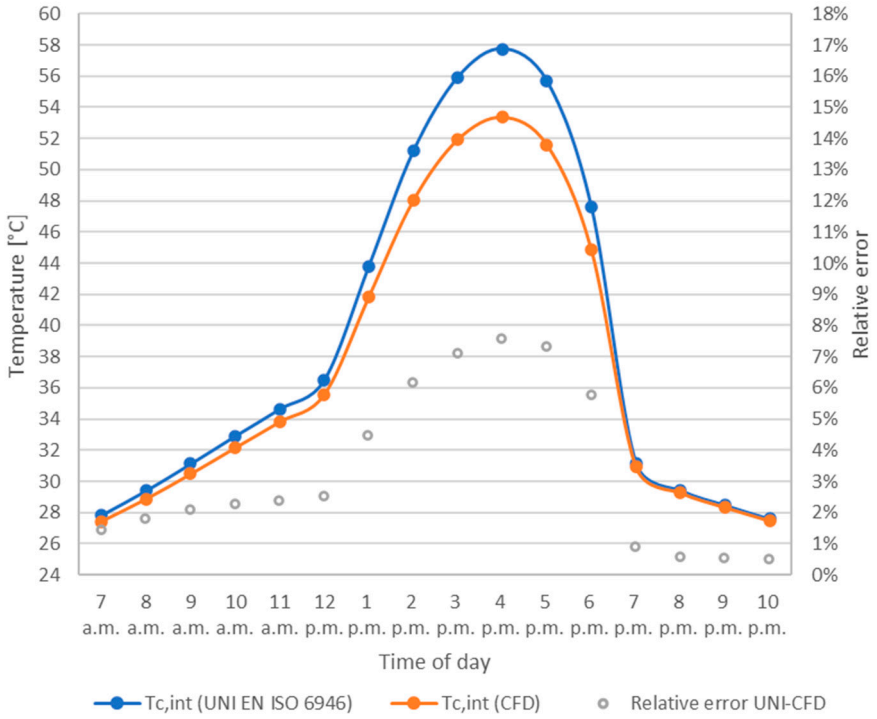

Figure 11. Comparison between the temperature values of the internal face of the cavity obtained by UNI EN ISO 6946 and by CFD. The graph shows also the RE of the CFD compared to the standard at each hour.

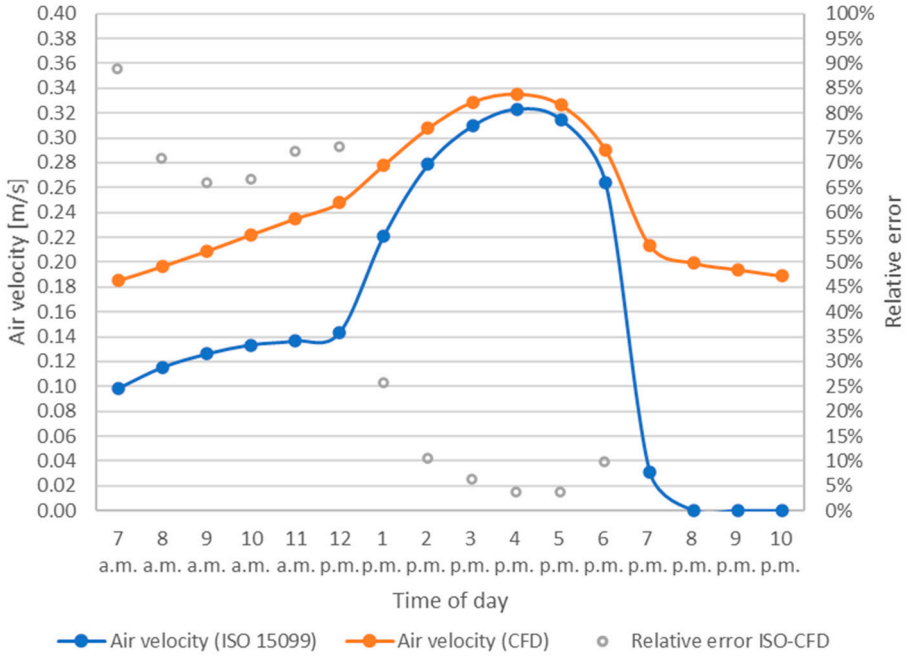

Figure 12. Comparison between the average air velocity values inside the naturally ventilated cavity calculated according to ISO 15099 and provided by the CFD simulations. The graph shows also the RE of the CFD compared to the standard, calculated until 6:00 p.m.

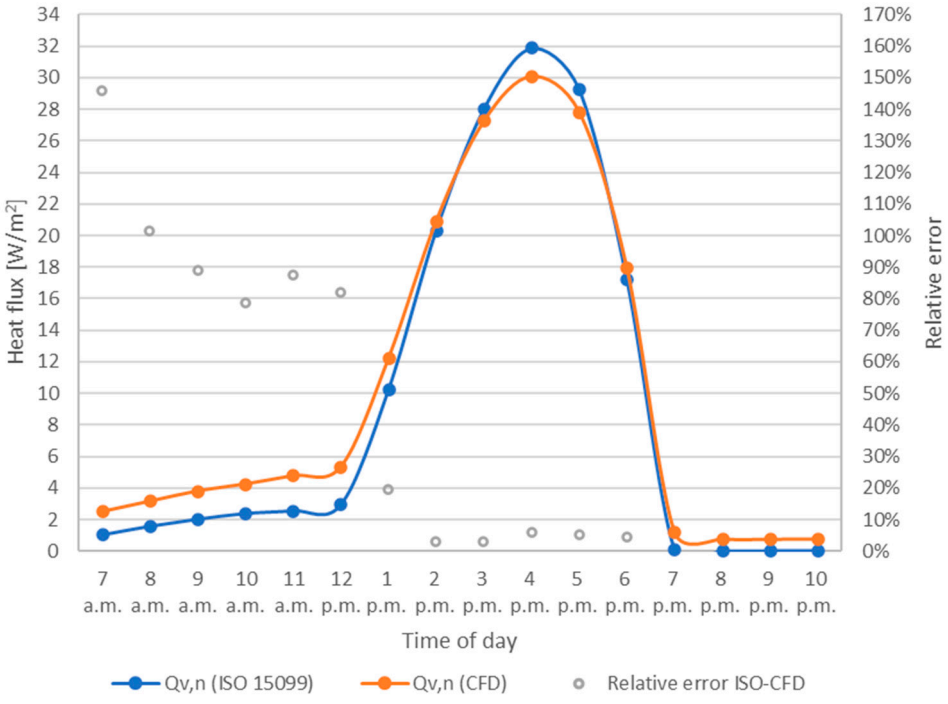

Figure 13. Comparison between the heat flux removed from the cavity by natural ventilation ($Q_{v,n}$) calculated according to ISO 15099 and CFD simulations. The graph shows also the RE of the CFD compared to the standard, calculated until 6:00 p.m. local results.

Figure 11 represents the temperature profile of the internal surface of the cavity ($T_{c,int}$) calculated according to UNI EN ISO 6946 and by CFD at each hour. The difference between the two curves is bigger during the hottest hours of the day, because of the standard procedure simplifications, as previously discussed for Figure 10. The MRE of the temperature values provided by CFD compared to UNI EN ISO 6946 is 3%.

Figure 12 shows the comparison between the average air velocity values inside the naturally ventilated cavity obtained following ISO 15099 and provided by the CFD simulations. The velocity value calculated using the standard was imposed equal to zero at 8:00, 9:00 and 10:00 p.m., when the temperature of the internal face of the cavity is lower than the external air temperature (T_e), because of the absence of incident solar radiation on the external surface of the façade. Hence, the Rayleigh number would be Ra < 0, for this reason it was assumed absence of convection into the cavity (convective heat transfer coefficient $h_{cv} = 0$, air velocity inside the cavity v = 0 and heat flux removed from the cavity $Q_{v,n} = 0$). The discrepancy between the velocity profiles in Figure 12 is related to all the assumptions of the calculation procedure followed (see Appendix A). In this case, the hourly RE was calculated until 6:00 p.m., in fact the air velocity value obtained by ISO 15099 between 7:00 p.m. and 10:00 p.m. is not accurate, because of the calculation methodology. The MRE of CFD values with respect to the standard is 41%.

Figure 13 describes the heat flux removed from the cavity by natural ventilation, always comparing the values obtained by CFD and by ISO 15099. As in the previous case, the RE was not evaluated after 6:00 p.m., when the heat flux tends or is equal to zero and the RE value would increase without physical meaning. The MRE of the CFD values with respect to the standard is 52%, while the maximum difference between the heat fluxes removed from the cavity is 2.4 W/m^2 at 12:00 p.m. The discrepancy between the profiles depends on the assumption made in the calculation procedure developed, but despite this the results regarding the heat flux $Q_{v,n}$ show a quite good level of agreement.

In conclusion, the quantities benchmarked show a very similar trend between CFD and standards. The computed RE reflects the assumptions that a normative cannot avoid making for the simplicity of its application. In particular, what influences the results the most is that the simulations consider a 3D temperature, velocity and pressure fields while the standards rely on 1D correlations that generally tend to overestimate the thermal performance of the cavity for safety reasons.

Once the global performance of the façade is analyzed, it might be useful to investigate the air behavior inside the cavity, in order to detect any possible criticality. This aspect is examined in this section. The considered case is the one referred to the 4:00 p.m. simulation results, since it is the time of the day with the greatest ventilation rate through the cavity. The boundary conditions considered for the simulation are: T_e = 33.49 °C, T_{sa} = 58.70 °C, and T_{duct} = 30.99 °C. The 2D air velocity profile in Figure 14 refers to a surface located inside the cavity, at half its thickness. In this case, the high external temperature and incident solar radiation contribute to reach a significant stack effect, with an air flow rate inside the cavity of 32 m^3/h. It is worth noting that the air velocity profile in the lower part of the cavity is very irregular: in fact the air flow enters the cavity with a velocity of about 3 m/s, creating stagnation vortexes on either side, and slows down rapidly along the façade height until a value of 0.40 m/s. This is caused by the geometry of the junction between the cavity and the duct, which does not allow a uniform expansion of the air jet inside the cavity. A wider cavity inlet section and a more gradual junction with the underground duct through a plenum would contribute to a better air flow distribution and a higher ventilation efficiency.

The temperature profile inside the cavity shown in Figure 15 reflects the velocity one: the benefits given by ventilation are limited to the lower half of the façade and, therefore, to the first floor of a hypothetical building equipped with this type of envelope. The average temperature on the internal face of the cavity is 50.51 °C between 0 and 4 m of height (corresponding to the building ground floor) and 55.45 °C between 4 and 8 m (building first floor).

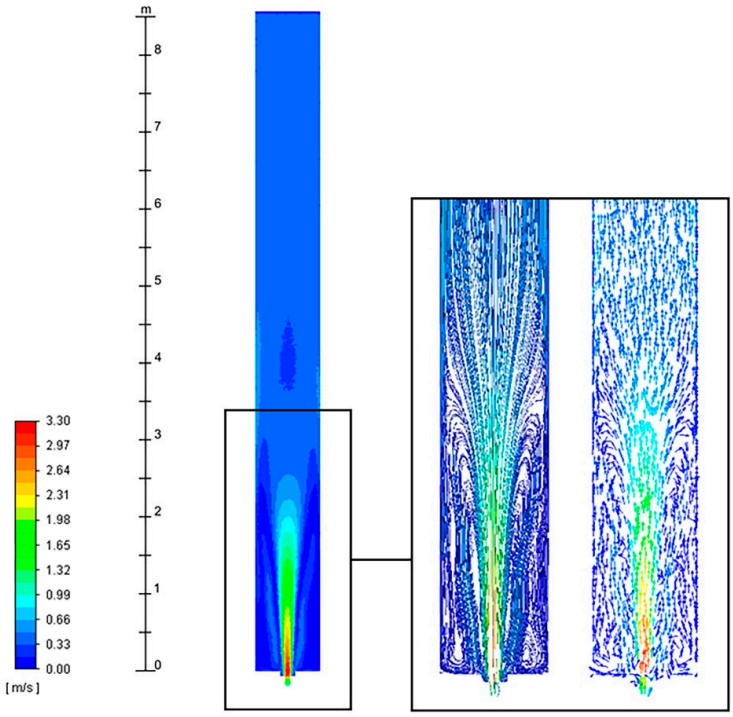

Figure 14. Air velocity profile inside the naturally ventilated cavity at 4:00 p.m., plotted on a surface at half the thickness of the cavity.

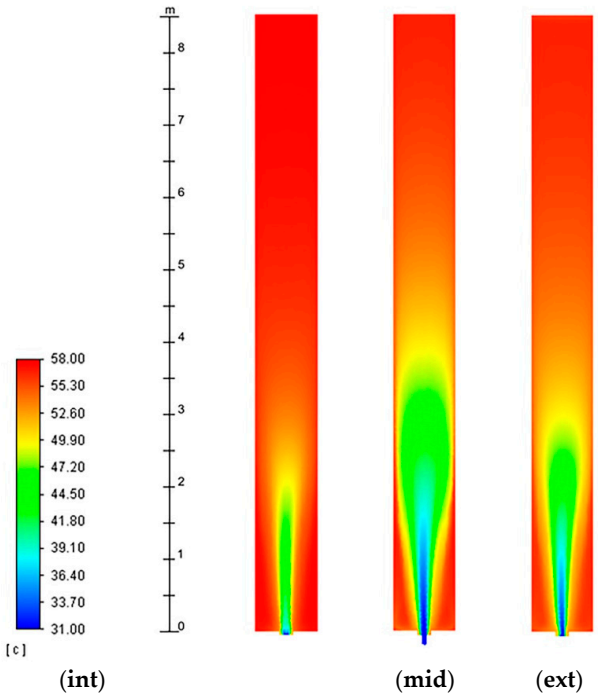

Figure 15. Temperature profile inside the naturally ventilated cavity at 4:00 p.m., plotted on the internal (**int**) and external (**ext**) surfaces of the cavity and on another surface (**mid**) at half its thickness.

3.2. Sensitivity Analysis: Effect of Absorption Coefficient

Once the ventilated façade behavior over the day had been investigated, a sensitivity analysis was carried out by varying the absorption coefficient of its external surface α from 0.8 to $\alpha = 0.4$, in order to evaluate the external surface color influence on the thermal performance of the system. For this analysis, the natural ventilation case is considered but

the temporal span is limited to the central hours of the day (12:00 p.m., 2:00 p.m., 4:00 p.m., and 6:00 p.m.), when the solar radiation reaches its maximum value and the absorption coefficient influence on the façade performance is the highest.

The results presented in Table 3 show a sensible reduction in the heat flux entering the cavity from the outside ($Q_{ext,n}$), thanks to the higher reflection of the external surface of the façade. Even if the air flow rate values inside the cavity are almost equal to the α = 0.8 case, there is a reduction in the heat flux removed from the cavity ($Q_{v,n}$). In fact, $Q_{v,n}$ is proportional to both the air flow rate and the air temperature variation between the inlet and the outlet of the cavity, which is much lower than in the case with α = 0.8. The most interesting quantity is the heat flux that enters the building ($Q_{int,n}$), which is significantly reduced after halving the absorption coefficient. The results obtained show almost a 40% reduction in the heat flux through the façade at 4:00 p.m., which confirms the importance of the façade color in limiting the building energy consumption during summer.

Table 3. Comparison between $Q_{ext,n}$, $Q_{v,n}$, and $Q_{int,n}$ values assuming α = 0.8 and α = 0.4.

Hour	**12:00 p.m.**		**2:00 p.m.**		**4:00 p.m.**		**6:00 p.m.**	
α	0.8	0.4	0.8	0.4	0.8	0.4	0.8	0.4
$Q_{ext,n}$ (W)	54.17	33.22	188.61	95.03	264.68	127.72	161.63	81.48
$Q_{v,n}$ (W)	38.37	20.23	152.11	70.80	219.24	97.88	130.42	61.23
$Q_{int,n}$ (W)	15.81	12.29	36.51	24.18	45.43	28.72	31.22	20.25
$\Delta Q_{int,n}$ %	22%		34%		37%		35%	

As previously done, it is interesting to look at the air flow inside the cavity in order to assess the influence of the absorbance coefficient modification. Once again, this aspect is examined referring to the 4:00 p.m. simulation results, with the following boundary conditions: T_e = 33.49 °C, T_{sa} = 46.10 °C, and T_{duct} = 30.99 °C. The resulting temperature profiles inside the cavity are reported in Figure 16: the absorption coefficient halving leads to a 10 °C temperature reduction on the cavity faces (the external and internal faces temperatures decrease respectively from 55.7 °C to 44.7 °C and from 53.4 to 43.4 °C) and to a better temperature uniformity along the façade height (and the different building floors).

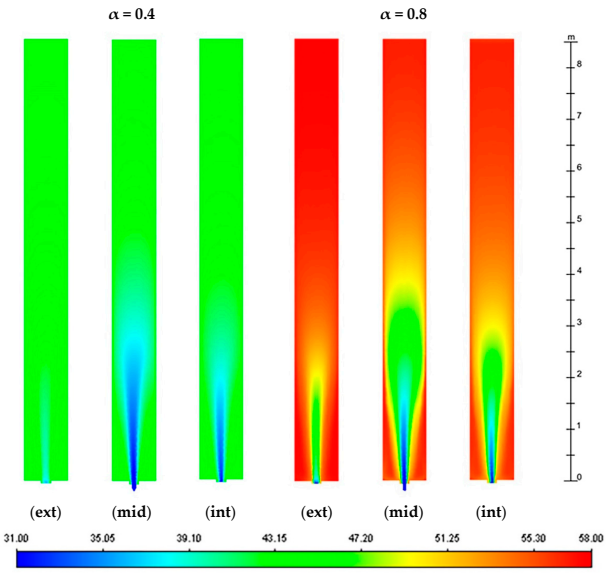

Figure 16. Comparison between the temperature profiles (indicated in °C) at 4:00 p.m. on the external (**ext**) and internal (**int**) surfaces of the ventilated cavity and on a surface (**mid**) at half its thickness, considering α = 0.4 and α = 0.8.

3.3. Energy Saving Analysis

The thermal behavior of a ventilated façade can be studied by introducing an indicator of performance, the energy saving rate S [29], which compares the ventilated and the unventilated façade (with closed cavity) behavior.

The energy saving rate S_i, due to the façade ventilation at each hour, has been defined as

$$S_i = \frac{Q_{nv,i} - Q_{int,n,i}}{Q_{nv,i}} \quad (10)$$

where $Q_{nv,i}$ and $Q_{int,n,i}$ are the heat fluxes that enter the building at a specific hour i, respectively referred to the unventilated and the ventilated façade.

The 24-h flux trend, referred to the façade with $\alpha = 0.8$, is reported in Figure 17: the heat flux through the unventilated façade is slightly higher than the one related to the ventilated façade, especially from 1:00 p.m. to 6:00 p.m., when the ventilation reaches its maximum efficiency. The chart in Figure 18 represents the hourly average energy saving rate (i.e., the average value along the façade height) that could be achieved thanks to natural ventilation in the cavity. On this graph, the blue columns indicate the percentage reduction of the incoming heat flux compared to the use of the unventilated façade ($1 - Q_{int,n,i}/Q_{nv,i}$), while the orange line represents the difference between the heat flux entering the building with closed cavity and with ventilated cavity ($Q_{nv,i} - Q_{int,n,i}$). Although, looking at the chart, it might seem that the efficiency of the ventilated façade is higher in the early morning hours than in the afternoon, a more careful analysis allows to verify the opposite, according to what expected. In fact, the ventilated façade provides a 18% reduction in the heat flux entering the building at 7:00 a.m., but since the heat fluxes involved are very small (Q_{nv} = 0.403 W/m^2 and $Q_{int,n}$ = 0.329 W/m^2), their difference is not relevant (0.1 W/m^2), as shown by the orange curve. On the other hand, at 4:00 p.m. the heat flux reduction is just 11%, but the difference between Q_{nv} and $Q_{int,n}$ is bigger than in the morning hours (0.75 W/m^2).

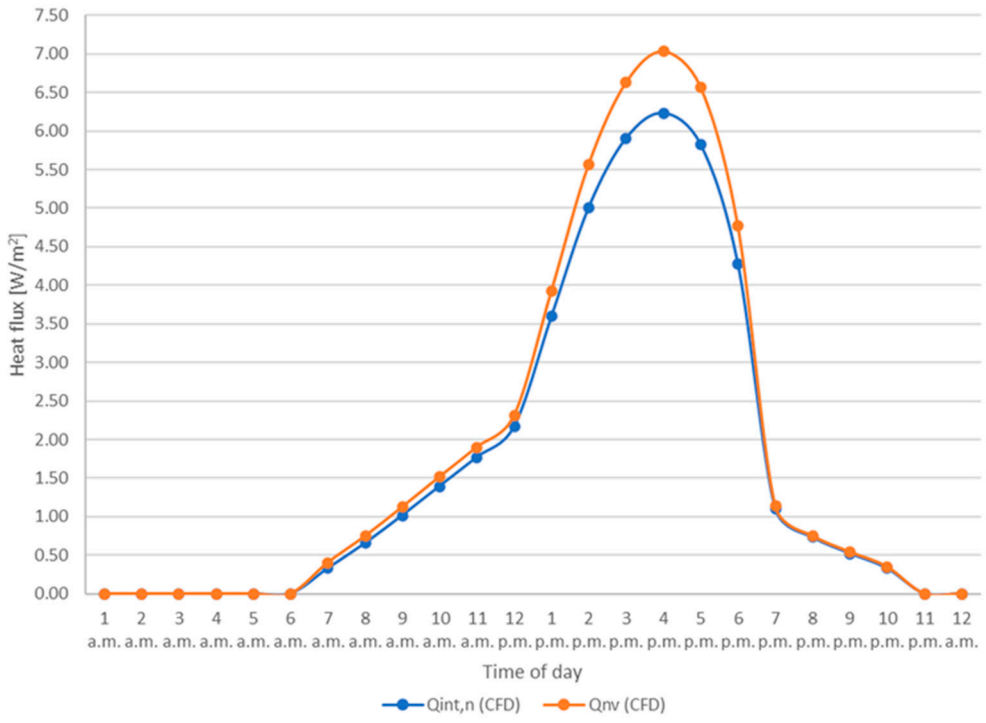

Figure 17. Comparison between the heat fluxes entering the building through the naturally ventilated façade ($Q_{int,n}$) and the unventilated façade (Q_{nv}).

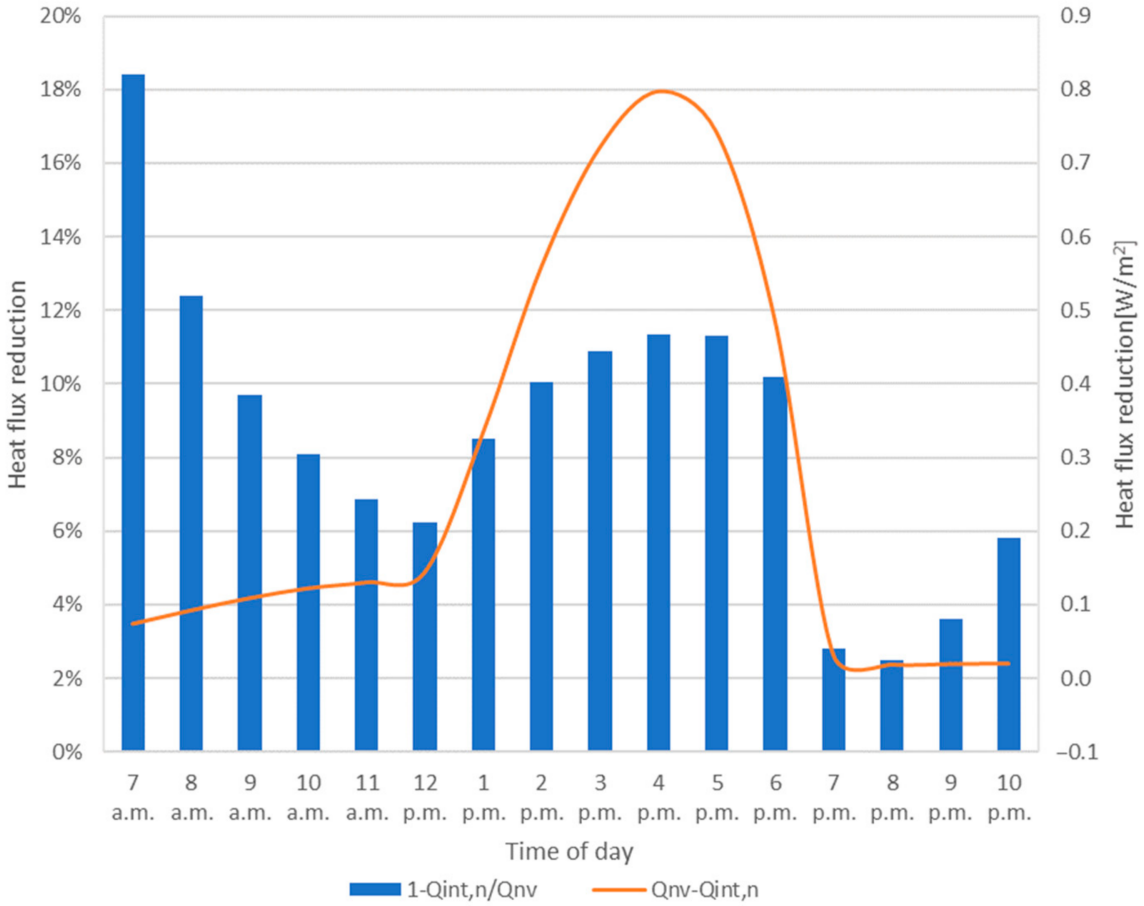

Figure 18. Hourly average energy saving (S_i) that could be reached using naturally ventilated façade instead of the unventilated one (the chart shows the average Si values along the façade height).

The daily energy saving rate S that could be achieved during summer thanks to the use of natural ventilation into the cavity, instead of the unventilated façade, can be written as

$$S = \sum_i S_i = 1 - \frac{\sum_i Q_{int,n,i}}{\sum_i Q_{nv,i}} \quad (11)$$

In the case studied, its value is approximately 10%.

However, looking at the average energy efficiency of the system, not considering the different benefits given by the ventilation depending on the façade height (as discussed in Section 3.2), could lead to a wrong building energy design. In fact, in the case studied, the heat flux $Q_{int,n}$ that enters the building is equal to 5.60 W/m^2 at the first floor level and 6.70 W/m^2 at the second floor level. This 1 W/m^2 difference in heat flux, multiplied by the whole building envelope area, can cause a significant discrepancy in thermal loads between the building floors, that could imply the installation of different cooling systems. The energy saving rate *Si* at 4:00 p.m., whose average is 11% (Figure 18), is actually equal to 19% for the first floor, and 4% for the second floor.

Hence, the evaluation of ventilated façades behavior considering the building height is very important, especially in case of high absorption coefficient values of the external surface and high incident solar radiation, while in case of low absorption coefficient values, and/or low incident solar radiation, the average behavior assessment could be considered accurate enough.

4. Conclusions

In this research, a 3D CFD model was developed in order to evaluate the energy performance of a timber–concrete composite prefabricated ventilated façade during summer and to compare the results obtained with the International Standards UNI EN ISO 6946 and ISO 15099. The study performed demonstrates the CFD potential and utility in studying a ventilated façade behavior, allowing detailed analysis, and an accurate system design. The international standards do not allow such detailed analysis, but they are easy to use and suitable for early design stages, as they can only assess the average behavior of the façade. However, the comparison with the simplified method proposed by UNI EN ISO 6946 and by ISO 15099 was essential to verify the CFD results consistency in absence of experimental results.

The simulations with closed cavity were used for the benchmark of the heat transfer model set in Fluent, by comparing the thermal resistance of the unventilated cavity obtained by the software with the one calculated according to UNI EN ISO 6946 and ISO15099.

The simulations concerning natural ventilation allowed to carry out a detailed evaluation of the façade performance over the day and to highlight its critical issues, that should be optimized. In this regard, it was possible to evaluate that:

- Solar radiation is the parameter that mostly affects the naturally ventilated façade performance, which achieves its maximum efficiency during the hottest hours of the day, characterized by the highest incident solar radiation values. This leads to a much lower efficiency during cloudy days and for shaded or north-facing façades.
- Geometry of the junction between the cavity and the underground duct is not optimal for a good air distribution in the lower part of the cavity; therefore, it would be advisable to widen the cavity inlet section and to insert a plenum.
- Natural ventilation allows to obtain energy benefits compared to the unventilated façade, however limited to the lower part of the façade (3–4 m of height) and therefore to the first floor of a hypothetical building with this type of envelope system. It is fundamental to consider the façade efficiency variation along its height for a correct building energy design, even if this aspect it is not taken into account by international standards.
- Color of the external surface of the façade significantly affects the envelope energy performance, since a 0.4 absorption coefficient value allows a heat flux reduction through the façade up to 40% compared to a 0.8 absorption coefficient value.

Forced ventilation allows an improvement in the energy performance of the façade during summer and decreases its dependency on climatic conditions, but requires fans to force the air inside the façade cavity, allowing a heat flux reduction through the building on one hand, and energy consumption and maintenance requirements on the other hand. The CFD model set for the case of forced ventilation could be used to evaluate the air velocity value that optimizes the overall building energy consumption, and the related cost, depending on the specific project.

The assumptions made in the CFD model implemented are in accordance with the research objective related to the comparison with the International Standards UNI EN ISO 6946 and ISO 15099. Future works should consider the implementation of air humidity and materials moisture content in the CFD model, in order to verify its influence on the façade thermal conductivity, and overall behavior. A more detailed description of the outdoor environment, including wind pressure effects, as well as the analysis of the concrete slab heat capacity and its influence on the thermal behavior of the ventilated façade system, both in summer and in winter, will be topics worthy of further study.

Author Contributions: Conceptualization, S.P. (Sofia Pastori), R.M., and E.S.M.; Methodology, S.P. (Sofia Pastori), R.M., E.S.M., S.P. (Stefano Passoni), and G.D.; Software, S.P. (Stefano Passoni); Validation, R.M. and S.P (Stefano Passoni); Formal analysis, S.P. (Sofia Pastori); Investigation, S.P. (Sofia Pastori); Resources, R.M., E.S.M., and S.P. (Stefano Passoni); Data curation, S.P. (Sofia Pastori); Writing—original draft preparation S.P. (Sofia Pastori) and E.S.M.; Writing—review and editing

R.M., E.S.M., and G.D.; Visualization, S.P. (Sofia Pastori); Supervision, E.S.M. and G.D.; Project administration, R.M. and E.S.M. All authors have read and agreed to the published version of the manuscript.

Funding: This research received no external funding.

Institutional Review Board Statement: Not applicable.

Informed Consent Statement: Not applicable.

Data Availability Statement: Data is contained within the article.

Conflicts of Interest: The authors declare no conflict of interest.

Appendix A

Table A1. Sun-air temperature values for Budoni (Italy) [28].

Orientation	South		East		North		West	
Hour \ α	0.8	0.4	0.8	0.4	0.8	0.4	0.8	0.4
1:00 a.m.	25.9	25.9	25.9	25.9	25.9	25.9	25.9	25.9
2:00 a.m.	25.5	25.5	25.5	25.5	25.5	25.5	25.5	25.5
3:00 a.m.	25.1	25.1	25.1	25.1	25.1	25.1	25.1	25.1
4:00 a.m.	24.9	24.9	24.9	24.9	24.9	24.9	24.9	24.9
5:00 a.m.	24.8	24.8	25.4	25.1	25.1	24.9	24.8	24.8
6:00 a.m.	26.4	25.7	41.3	33.1	30.3	27.6	26.4	25.7
7:00 a.m.	28.0	26.7	49.1	37.2	31.0	28.2	27.9	26.6
8:00 a.m.	30.2	28.2	51.4	38.8	29.8	28.0	29.5	27.8
9:00 a.m.	35.6	31.5	50.4	38.9	31.4	29.4	31.3	29.3
10:00 a.m.	41.0	34.9	47.2	37.9	33.1	30.9	33.1	30.9
11:00 a.m.	44.1	37.2	42.4	36.3	34.9	32.6	34.9	32.6
12:00 p.m.	46.3	39.0	36.8	34.3	36.4	34.1	36.8	34.3
1:00 p.m.	46.6	39.7	37.4	35.1	37.4	35.1	44.3	38.5
2:00 p.m.	45.8	39.6	37.9	35.7	37.9	35.7	51.9	42.7
3:00 p.m.	42.0	37.9	37.7	35.7	37.8	35.8	56.8	45.3
4:00 p.m.	37.5	35.5	36.8	35.1	37.1	35.3	58.7	46.1
5:00 p.m.	35.5	34.2	35.3	34.1	38.5	35.7	56.5	44.7
6:00 p.m.	33.3	32.6	33.3	32.6	37.2	34.5	48.2	40.0
7:00 p.m.	30.8	30.7	30.8	30.7	31.1	30.9	31.3	31.0
8:00 p.m.	29.5	29.5	29.5	29.5	29.5	29.5	29.5	29.5
9:00 p.m.	28.5	28.5	28.5	28.5	28.5	28.5	28.5	28.5
10:00 p.m.	27.6	27.6	27.6	27.6	27.6	27.6	27.6	27.6
11:00 p.m.	26.9	26.9	26.9	26.9	26.9	26.9	26.9	26.9
12:00 p.m.	26.4	26.4	26.4	26.4	26.4	26.4	26.4	26.4

Table A2. Material properties considered for the model.

Material	Properties
Air	- variable density as function of temperature (incompressible ideal gas) - specific heat at constant pressure c_p = 1006.43 J/kg·K - thermal conductivity λ = 0.0242 W/m·K - dynamic viscosity μ = $1.7894 \cdot 10^{-5}$ Pa·s - molar mass Mm = 28.966 kg/kmol
Concrete	- density ρ = 2400 kg/m^3 - specific heat at constant pressure c_p = 653 J/kg·K - thermal conductivity λ = 2 W/m·K - emissivity ε = 0.9
Timber-frame	- density ρ = 100 kg/m^3 * - specific heat at constant pressure c_p = 1030 J/kg·K - thermal conductivity λ = 0.052 W/mK ** - emissivity ε = 0.8

* Coinciding with the rockwool density; ** Area weighted average value of wood and rockwool, coherently with UNI EN ISO 6946.

Table A3. Model set-up.

Operating Conditions	
Operating pressure	Atmospheric pressure (101325 Pa)
Operating density	1.225 kg/m^3
Gravitational acceleration	9.81 m/s^2
Turbulence Model	
Model	k-ε Realizable
Model constants	Default
Near-wall treatment	Enhanced wall treatment
Options	Full buoyancy effects
Radiation Model	
Model	Discrete Ordinates (DO)
Angular discretization	Theta, Phi: 3
Energy iterations per radiation iteration	10
Solver	
Type	Pressure-based
Pressure-velocity coupling	Coupled
Spatial discretization	Gradient: Green-Gauss node based Pressure: PRESTO! Other equations: second order upwind
Under relaxation factors	Default
Temporal analysis	Steady Pseudo transient
Options	Warped-face gradient correction High order term relaxation

Table 4. Values of the delta temperature between the cavity faces, heat flux through the cavity and thermal resistance of the cavity obtained from the CFD simulations for the closed cavity; comparison with the thermal resistance values calculated according to ISO 15099 and UNI EN ISO 6946. The relative error (RE) indicates the difference of the CFD results from the standards.

Time of Day	Temperature Difference ΔT (K)	Heat Flux Q_{nv} (W/m^2)	Thermal Resistance Closed Cavity R_g (m^2K/W)				
			CFD	ISO 15099	RE ISO-CFD	UNI EN ISO 6946	RE UNI-CFD
7:00 a.m.	0.074	0.403	0.184	0.188	2%	0.180	2%
8:00 a.m.	0.135	0.747	0.181	0.185	2%	0.180	1%
9:00 a.m.	0.201	1.126	0.178	0.183	2%	0.180	1%
10:00 a.m.	0.266	1.518	0.176	0.180	2%	0.180	2%
11:00 a.m.	0.329	1.901	0.173	0.177	2%	0.180	4%
12:00 p.m.	0.394	2.313	0.170	0.175	2%	0.180	5%
1:00 p.m.	0.629	3.929	0.160	0.164	3%	0.180	11%
2:00 p.m.	0.839	5.569	0.151	0.154	3%	0.180	16%
3:00 p.m.	0.960	6.627	0.145	0.149	2%	0.180	20%
4:00 p.m.	0.956	7.032	0.143	0.146	2%	0.180	21%
5:00 p.m.	0.954	6.570	0.145	0.149	2%	0.180	19%
6:00 p.m.	0.740	4.770	0.155	0.159	3%	0.180	14%
7:00 p.m.	0.203	1.141	0.178	0.183	2%	0.180	1%
8:00 p.m.	0.136	0.754	0.181	0.185	2%	0.180	1%
9:00 p.m.	0.099	0.542	0.183	0.187	2%	0.180	1%
10:00 p.m.	0.064	0.350	0.184	0.188	2%	0.180	2%

Table 5. Thermal transmittance calculation for the opaque ventilated façade following UNI EN ISO 6946.

Layer	Thickness (m)	Thermal Conductivity (W/mK)	Thermal Resistance (m^2K/W)
Thermal resistance inner surface	-	-	0.130 *
OSB panel	0.015	0.100	0.150
Timber-frame	0.200		
Rockwool panel	0.200	0.049 **	4.061
OSB panel	0.009	0.100	0.090
Ventilated air cavity	0.031	-	0.130 *
Reinforced concrete slab	0.050	-	-
Thermal resistance outer surface	-	-	-
Total thermal resistance (m^2K/W)			4.561
Thermal transmittance (W/m^2K)			0.219

* Value from UNI EN ISO 6946; ** Weighted average of timber and rockwool thermal conductivities.

Thermal Resistance Calculation Procedure for the Ventilated Cavity Using ISO 15099

Starting from the $Q_{int,n}$ values calculated by UNI EN ISO 6946, it is possible to obtain the temperature of the internal surface of the naturally ventilated cavity ($T_{c,int}$) at each hour. According to [32] for vertical symmetrically heated, isothermal plates, it is possible to calculate the Rayleigh Number using the following semiempirical correlation

$$Ra = \frac{g\,\beta\,(T_{c,int} - T_\infty)d^3}{\alpha\,\nu} \quad (A1)$$

where g is the gravitational acceleration, β is the air thermal expansion coefficient, d is the cavity thickness, $T_{c,int}$ is the temperature of its internal face, T_∞ is the undisturbed flow temperature (considered equal to the external temperature T_e), α is the air thermal

diffusivity and ν is the air kinematic viscosity. The Nusselt number correlation applicable for isothermal conditions [33] is of the form

$$\mathrm{Nu} = \left[\frac{C_1}{(\mathrm{Ra}\ d/H)^2} + \frac{C_2}{(\mathrm{Ra}\ d/H)^{1/2}} \right]^{-1/2} \quad \text{(A2)}$$

where C_1 = 576, C_2 = 2.87, and H is the façade height (8.5 m).

The previous correlations refer to a ventilated cavity between two parallel isothermal surfaces, but since in the case studied the delta temperature between the external and internal surfaces of the ventilated cavity is little (with maximum value of ΔT = 2.33 °C at 4:00 p.m.), the error introduced is not considered relevant. The Nusselt number values are then used to calculate the convective heat transfer coefficient h_{cv} [33] of the air flow into the cavity at each hour

$$h_{cv} = \frac{\mathrm{Nu}\ \lambda}{d} \quad \text{(A3)}$$

where λ is the air thermal conductivity.

Once the h_{cv} values are known it is possible to calculate the air velocity inside the ventilated cavity and the heat flux $Q_{v,n}$ following the ISO 15099 procedure concerning thermally-driven ventilation.

Table 6. Hourly values of the heat flux through the façade ($Q_{int,n}$), temperature of the internal cavity face ($T_{c,int}$), convective coefficient inside the cavity (h_{cv}), air velocity inside the cavity (v), and heat flux removed from the cavity ($Q_{v,n}$).

Hour	T_e (°C)	$Q_{int,n}$ (W/m^2)	$T_{c,int}$ (°C)	h_{cv} (W/m^{2}K)	v (m/s)	$Q_{v,n}$ (W)
7:00 a.m.	25.39	0.41	27.83	0.642	0.10	7.36
8:00 a.m.	26.20	0.77	29.40	0.767	0.12	11.34
9:00 a.m.	27.37	1.16	31.12	0.843	0.13	14.59
10:00 a.m.	28.72	1.56	32.90	0.895	0.13	17.21
11:00 a.m.	30.25	1.95	34.64	0.916	0.14	18.48
12:00 p.m.	31.69	2.37	36.50	0.960	0.14	21.24
1:00 p.m.	32.77	4.02	43.80	1.368	0.22	74.22
2:00 p.m.	33.49	5.68	51.18	1.591	0.28	147.49
3:00 p.m.	33.76	6.75	55.92	1.697	0.31	203.52
4:00 p.m.	33.49	7.16	57.74	1.739	0.32	231.50
5:00 p.m.	32.86	6.70	55.67	1.711	0.31	212.49
6:00 p.m.	31.87	4.87	47.59	1.538	0.26	124.84
7:00 p.m.	30.70	1.17	31.19	0.158	0.03	0.44
8:00 p.m.	29.53	0.77	29.43	0 *	0	0
9:00 p.m.	28.54	0.56	28.47	0 *	0	0
10:00 p.m.	27.64	0.36	27.59	0 *	0	0

* This value has been imposed equal to zero because $T_{c,int} < T_e$, due to the absence of incident solar radiation on the external surface of the façade, therefore the Rayleigh number would be Ra < 0. For this reason, it was assumed absence of convection into the façade cavity at 8:00, 9:00 and 10:00 p.m. (h_{cv} = 0, v = 0, $Q_{v,n}$ = 0).

References

1. Transforming Our World: The 2030 Agenda for Sustainable Development, A/RES/70/1, 2015, United Nations. Available online: https://sustainabledevelopment.un.org/post2015/transformingourworld/publication (accessed on 1 June 2020).
2. Sánchez, M.N.; Giancola, E.; Blanco, E.; Soutullo, S.; Suárez, M.J. Experimental Validation of a Numerical Model of a Ventilated Façade with Horizontal and Vertical Open Joints. *Energies* **2020**, *13*, 146. [CrossRef]
3. Ciampi, M.; Leccese, F.; Tuoni, G. Ventilated facades energy performance in summer cooling of buildings. *Sol. Energy* **2003**, *75*, 491–502. [CrossRef]
4. Akbari, H.; Konopacki, S.; Pomerantz, M. Cooling energy savings potential of reflective roofs for residential and commercial buildings in the United States. *Energy* **1999**, *24*, 391–407. [CrossRef]

5. Francés, V.; Escriva, E.J.; Ojer, J.; Bannier, E.; Soler, V.; Moreno, G. Modeling of ventilated façades for energy building simulation software. *Energy Build.* **2013**, *65*, 419–428. [CrossRef]
6. Simo-Tagne, M.; Chinenye Ndukwu, M.; Rogaume, Y. Modelling and numerical simulation of hygrothermal transfer through a building wall for locations subjected to outdoor conditions in Sub-Saharan Africa. *J. Build. Eng.* **2019**, *26*, 100901. [CrossRef]
7. Danovska, M.; Pernigotto, G.; Baggio, P.; Gasparella, A. Assessment of the thermal performance of timber walls under nominal or moisture and temperature dependent properties. In Proceedings of the 16th IBPSA Conference, Rome, Italy, 2–4 September 2019; pp. 508–515. [CrossRef]
8. Destro, R.; Boscato, G.; Mazzali, U.; Russo, S.; Peron, F.; Romagnoni, P. Structural and thermal behaviour of a timber-concrete prefabricated composite wall system. *Energy Procedia* **2015**, *78*, 2730–2735. [CrossRef]
9. Souza, L.C.O.; Souza, H.A.; Rodrigues, E.F. Experimental and numerical analysis of a naturally ventilated double-skin façade. *Energy Build.* **2018**, *165*, 328–339. [CrossRef]
10. Zhang, T.; Yang, H. Flow and heat transfer characteristics of natural convection in vertical air channels of double-skin solar façades. *Appl. Energy* **2019**, *242*, 107–120. [CrossRef]
11. Coussirat, M.; Guardo, A.; Jou, E.; Egusquiza, E.; Cuerva, E.; Alavedra, P. Performance and influence of numerical sub-models on the CFD simulation of free and forced convection in double-glazed ventilated facades. *Energy Build.* **2008**, *40*, 1781–1789. [CrossRef]
12. Nore, K.; Blocken, B.; Thue, J.V. On CFD simulation of wind-induced airflow in narrow ventilated facade cavities: Coupled and decoupled simulations and modelling limitations. *Build. Environ.* **2010**, *45*, 1834–1846. [CrossRef]
13. *UNI EN ISO 6946:2018 Componenti ed Elementi per Edilizia—Resistenza Termica e Trasmittanza Termica—Metodi di Calcolo*; UNI—Ente Italiano di Normazione: Milan, Italy, 2018.
14. *ISO 15099:2003 Thermal Performance of Windows, Doors and Shading Devices—Detailed Calculations*; International Organization for Standardization: Geneva, Switzerland, 2003.
15. Arkar, C.; Domjan, S.; Medved, S. Lightweight composite timber façade wall with improved thermal response. *Sustain. Cities Soc.* **2018**, *38*, 325–332. [CrossRef]
16. Fruehwald, A.; Knauf, M. Carbon aspects promote building with wood. In Proceedings of the World Conference on Timber Engineering, Quebec City, QC, Canada, 10–14 August 2014.
17. Brandner, R. Production and Technology of Cross Laminated Timber (CLT): A state-of-the-art Report. In Proceedings of the Focus Solid Timber Solutions—European Conference on Cross Laminated Timber, Graz, Austria, 21–22 May 2013; pp. 3–36.
18. Lehmann, S. Wood in the Urban Context: Infill Development Using Prefabricated Timber Construction Systems. In Proceedings of the CIB WBC, Brisbane, Australia, 5–9 May 2013.
19. Mikkola, M. Industrial approach to wood based multistory construction—Case Stora Enso modular construction. In Proceedings of the 20 Internationales Holzbau Forum IHF, Garmisch-Partenkirchen, Germany, 3–5 December 2014.
20. Pastori, S. Aria® Constructive System: CFD Analysis for the Energy Performance Optimization and Life Cycle Assessment. Master's Thesis, Politecnico di Milano, Milan, Italy, 2020.
21. *UNI 10351:2015 Materiali e Prodotti per Edilizia—Proprietà Termoigrometriche—Procedura per la Scelta dei Valori di Progetto*; UNI—Ente Italiano di Normazione: Milan, Italy, 2015.
22. Inventory of Carbon & Energy (ICE). *Version 2.0, Sustainable Energy Research Team (SERT)*; Department of Mechanical Engineering, University of Bath: Bath, UK, 2011.
23. Steeman, M.; Himpe, E.; Vanroelen, M.; Roeck, M. *Environmental Impact of Timber Frame Walls*; IOP Conference Series: Earth and Environmental Science; IOP Publishing: Bristol, UK, 2019. [CrossRef]
24. Using Thermal Mass in Timber-Framed Buildings—Effective Use of Thermal Mass for Increased Comfort and Energy Efficiency. 2015. Available online: https://www.woodsolutions.com.au/system/files/WS_TDG23_Therm_Mass_TFB_July2015.pdf (accessed on 5 June 2020).
25. ANSYS Fluent Theory Guide. Available online: https://www.afs.enea.it/project/neptunius/docs/fluent/html/th/main_pre.htm (accessed on 16 September 2020).
26. Dama, A.; Angeli, D.; Larsen, O.K. Naturally ventilated Double-Skin Façade in Modeling and Experiments. *Energy Build.* **2017**, *144*, 17–29. [CrossRef]
27. Gagliano, A.; Patania, F.; Ferlito, A.; Nocera, F.; Galesi, A. Computational Fluid Dynamic Simulations of Natural Convection in Ventilated Facades. *Evaporation Condens. Heat Transf.* **2011**, 349–374. [CrossRef]
28. *UNI 10349-1:2016 Riscaldamento e Raffrescamento Degli Edifici—Dati Climatici—Parte 1: Medie Mensili per la Valutazione della Prestazione Termo-Energetica Dell'Edificio e Metodi per Ripartire L'Irradianza Solare Nella Frazione Diretta e Diffusa e per Calcolare L'Irradianza Solare su di Una Superficie Inclinata*; UNI—Ente Italiano di Normazione: Milan, Italy, 2016.
29. Patania, F.; Gagliano, A.; Nocera, F.; Ferlito, A.; Galesi, A. Thermofluid-dynamic analysis of ventilated facades. *Energy Build.* **2010**, *42*, 1148–1155. [CrossRef]
30. Lambie, E.; Saelens, D. Identification of the Building Envelope Performance of a Residential Building: A Case Study. *Energies* **2020**, *13*, 2469. [CrossRef]
31. Sistemi Geotermici a Bassa Temperatura: Caratteristiche e Opportunità. Technical Guide Issued by Consiglio Nazionale dei Geologi. 2014. Available online: http://www.cngeologi.it/wp-content/uploads/2014/12/GeologiInfo_Sistemi-geotermici-a-bassa-temperatura.pdf (accessed on 1 October 2020).

32. Baldinelli, G. A methodology for experimental evaluations of low-e barriers thermal properties: Field tests and comparison with theoretical models. *Build. Environ.* **2010**, *45*, 1016–1024. [CrossRef]
33. Incropera, F.P.; DeWitt, D.P.; Bergman, T.L.; Lavine, A.S. *Fundamentals of Heat and Energy Mass Transfer*, 6th ed.; John Wiley & Sons: Hoboken, NJ, USA, 2006; pp. 585–586.